Journal of Sound and Vibration 329 (2010) 2915–2927

Contents lists available at ScienceDirect

Journal of Sound and Vibration

journal homepage: www.elsevier.com/locate/jsvi

Influence of hood geometry on the compression wave generated by a high-speed train

P.R. Murray *, M.S. Howe

Boston University, College of Engineering, 110 Cummington Street, Boston, MA 02215, USA

ARTICLE INFO

Article history:
Received 27 September 2009
Received in revised form
28 January 2010
Accepted 29 January 2010
Handling Editor: A.V. Metrikine
Available online 18 February 2010

ABSTRACT

A compression wave is generated when a high-speed train enters a tunnel. The wave propagates ahead of the train at the speed of sound. In a long tunnel nonlinear steepening of the wavefront produces the emission of a strong *micro-pressure wave* (mpw) from the distant tunnel exit. The mpw can produce structural damage to the tunnel and rattles in surrounding buildings. Nonlinear steepening can be countered by increasing the initial rise time of the compression wave by installing a tunnel entrance 'hood' consisting of a nominally uniform extension of the tunnel of larger cross-section. In this paper a theoretical examination is made of the influence on the wave of the rapid change in tunnel cross-section in the transition region between the tunnel and hood. It is shown that by optimally profiling the cross-sectional area changes across this region it is possible to minimize the amplitudes of second and third peaks of the compression wave pressure gradient. By this means the amplitudes of the secondary peaks in the micro-pressure wave are greatly reduced.

© 2010 Elsevier Ltd. All rights reserved.

1. Introduction

The compression wave generated when a high-speed train enters a tunnel propagates ahead of the train at the speed of sound [1–6]. The profile of the wavefront is known to depend on the shape of the train nose and on the geometry of the tunnel portal [7–13]. The pressure rise across the wavefront increases rapidly with train speed, and can often exceed 3% of atmospheric pressure [14,15]. In long tunnels its arrival at the distant tunnel exit results in the radiation of a loud, pulsatile 'bang', called the *micro-pressure wave* (mpw), that produces 'rattles' and vibrations in neighboring buildings. The environmental consequences of the mpw are particularly significant for long tunnels with acoustically smooth concrete slab tracks, which tend to promote nonlinear steepening of the wavefront. In this case the bang is very similar in amplitude to the sonic-boom from a supersonic aircraft.

It has been found [7,8,14–17] that the most effective way to suppress nonlinear wave steepening is by installation of a tunnel entrance 'hood'. In its simplest form the hood consists of a thin-walled, cylindrical extension (up to 50 m or more) ahead of the tunnel portal with uniform cross-sectional area $\mathcal{A}_h$ that exceeds the tunnel cross-section $\mathcal{A}$, say. Multiple reflections from opposite ends of the hood temporarily trap compression wave energy within the hood and thereby produce a large increase in the thickness of the compression wavefront, but with a 'rippled' profile. The subsequent nonlinear steepening of the wavefront is effectively opposed provided a sufficiently large increase in the initial wavefront thickness can be achieved. This is illustrated schematically in Figs. 1 and 2, which show the compression waveforms within

* Corresponding author. Present address: Department of Mathematics, Keele University, ST5 5AX, UK. Tel.: +44 7545035011.
E-mail address: p.r.murray@keele.ac.uk (P.R. Murray).

0022-460X/$ - see front matter © 2010 Elsevier Ltd. All rights reserved.
doi:10.1016/j.jsv.2010.01.036

Nomenclature

$\mathcal{A}$	cross-sectional area of tunnel
$\mathcal{A}_h$	cross-sectional area of hood
$\mathcal{A}_0$	uniform cross-sectional area of train
$\mathcal{A}_T$	cross-sectional area of train nose
c_0	mean sound speed in tunnel
G	Green's function (4)
h	uniform radius of model train
H(x)	Heaviside unit step function
L	length of nose
ℓ_h	length of hood
ℓ'	length end correction
M	train Mach number
p	compression wave pressure
R	tunnel radius
R_h	hood radius
$\mathcal{R}_E$	open end reflection coefficient
$\mathcal{R}_J$	junction reflection coefficient
$r=f(x)$	transition profile function
r_n	radial transition node n
$\mathcal{T}_J$	junction transmission coefficient
s	distance measured from nose tip
t	time
$[t]$	retarded time
U	train speed
(x,y,z)	coordinate axes
$\mathbf{x}$	(x,y,z)
x_n	axial transition node n
$\delta(x)$	Dirac delta function
ρ_0	mean air density
φ_E^*	potential flow function for hood portal
φ_J^*	potential flow function for the junction

the tunnel and the resulting mpw pulse shapes for a tunnel with and without a hood. The strength of the mpw is approximately proportional to the 'pressure gradient' $\partial p/\partial t$, the partial time derivative of the compression wave pressure p near the tunnel exit [5,8]. Thus the reduced value of the maximum pressure gradient for the elongated compression wave produced by the hood tends to weaken the variable micro-pressure wave amplitude relative to its value in the absence of the hood.

Additional modifications of the initial compression wave profile can be effected by venting high pressure air in front of the advancing train through a series of 'windows' or other perforations in the hood walls [14,15,18–20], or by flaring or scarfing the tunnel portal [19,21,22]. Such modifications are usually studied by means of experiments performed at model scale [14,15], although it is now possible to perform preliminary design studies by rapid computer simulation [18]. In this paper waveform refinements are examined that can be produced by suitably profiling the otherwise discontinuous jump in cross-sectional area (from $\mathcal{A}_h$ to $\mathcal{A}$) at the junction of a uniform, unvented hood and the tunnel. Wave trapping in the hood depends on reflections from this junction, but there is also a contribution from the junction to compression wave formation during the passage of the train nose from the hood into the tunnel [18]. It might therefore be anticipated that the provision of some sort of optimal continuous modification of the existing geometry between the hood and the tunnel can

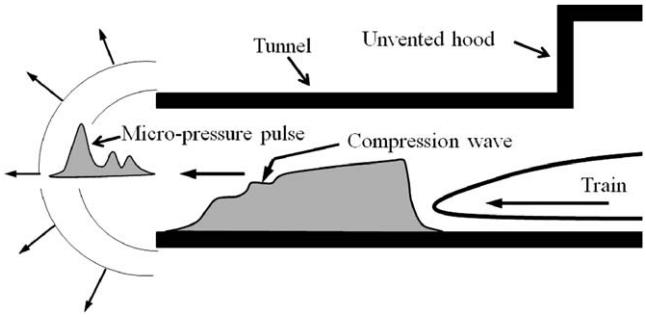

Fig. 1. Schematic illustration of the compression wave and corresponding micro-pressure pulse produced by a train entering a tunnel with a uniform hood.

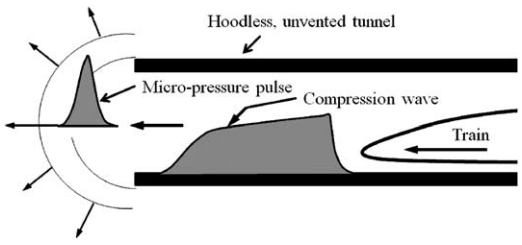

Fig. 2. Schematic illustration of the compression wave and corresponding micro-pressure pulse produced by a train entering a tunnel with no hood.

lead to a reduction in the subjective effects of the secondary peaks of $\partial p/\partial t$ (corresponding roughly to the secondary peaks of the mpw of Fig. 1).

With the notable exception of the flared portal [19,21], there have hitherto been no investigations of a hood with smoothly variable interior geometry. The first peak of the pressure gradient is produced by the first interaction between the hood portal and the train nose [18], and is therefore not affected by geometrical modification at the junction. However, junction geometry is likely to affect significantly both the positions and magnitudes of the second and third peaks of $\partial p/\partial t$. To investigate this a numerical scheme is described in this paper for the rapid evaluation of a large ensemble of candidate transition geometries. The optimum transition geometry is defined as that which minimizes the values of the second and third peaks in $\partial p/\partial t$.

The calculations are performed for the train speeds U = 250, 300, 350 km/h. To do this the numerical procedure applies the aeroacoustic theory discussed and extensively validated against experiment in [18]. This is based on the use of an aeroacoustic Green's function tailored to the hood geometry first introduced in [23]. For each candidate geometry Green's function must be evaluated from a preliminary calculation involving a numerical solution of Laplace's equation. The relevant aeroacoustic theory is outlined in Section 2 and discussed in relation to experiment in Section 3, where the principal components of the pressure gradient profile are identified. The optimization problem is formulated and solved in Sections 4 and 5.

2. Theory of compression wave formation

2.1. The aeroacoustic equation

Let p, ρ and c respectively denote the pressure, density, and speed of sound of the air. The Reynolds number in practice is sufficiently large for the initial flow during the passage of the train nose into the hood and tunnel to be regarded as inviscid and for the corresponding thermal losses to be negligible [24]. The sound generated by the interaction between the train and tunnel is therefore governed by the vortex sound equation for homentropic flow [18,25]

$$\left(\frac{D}{Dt}\left(\frac{1}{c^2}\frac{D}{Dt}\right)-\frac{1}{\rho}\nabla\cdot(\rho\nabla)\right)B=\frac{1}{\rho}\mathrm{div}\,(\rho\boldsymbol{\omega}\wedge\mathbf{v}), \tag{1}$$

where $B=\int \mathrm{d}p/\rho+\frac{1}{2}v^2$ is the total enthalpy, $\boldsymbol{\omega}=\mathrm{curl}\,\mathbf{v}$ is the vorticity and $\mathbf{v}$ is the velocity of the flow. Prior to the interaction B may be assumed constant throughout the fluid. In the region ahead of the train the air is regarded as linearly perturbed from its undisturbed state, and we can put $B\approx p/\rho_0$, where here and henceforth p will denote the linearly perturbed pressure and ρ_0 is the undisturbed air density.

The calculations will be performed for an axisymmetric tunnel-hood configuration involving a circular cylindrical tunnel of radius $R=(\mathcal{A}/\pi)^{1/2}$ fitted with a uniform hood of radius $R_h=(\mathcal{A}_h/\pi)^{1/2}$, where $R_h>R$. In the unmodified form the cross-sectional area changes abruptly at the junction, as indicated in Fig. 3. The origin of a rectangular coordinate system $\mathbf{x}=(x,y,z)$ is taken at the center of the hood entrance plane, with the negative x-axis extending along the common axis of the tunnel and hood. The train is modelled as a slender axisymmetric body that has cross-sectional area $\mathcal{A}_0$ over its uniform section. We consider only the simplest case of a train travelling coaxially into the tunnel, in the negative x-direction at constant speed U.

This idealized model corresponds to a typical experimental configuration usually adopted in compression wave studies [14,15]. There are, of course, significant differences between a 'real' tunnel and a bench-top experiment of this kind. However, during the initial stages of compression wave formation and propagation, when frictional effects can be neglected, especially those at ground level beneath the train, the real configuration is approximately dynamically equivalent to the cylindrical model consisting of the tunnel and train and their images in the ground plane.

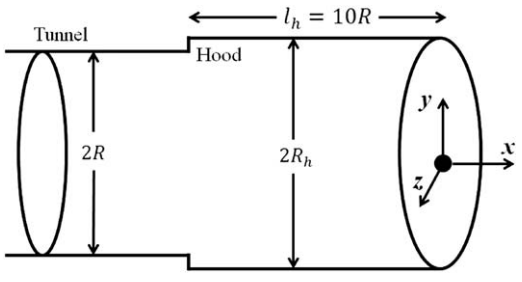

Fig. 3. Typical model-scale tunnel geometry consists of a circular cylindrical tunnel and hood sections of radius R, R_h, respectively. The coordinate origin is at the center of the hood entrance plane.

2.2. Representation of the moving train

In the acoustic region ahead of the train the air is initially only linearly perturbed from its undisturbed state so that, because B is constant in the absence of the train, the wave operator on the left hand side may be linearized by replacing the density ρ and sound speed c by their respective mean values ρ_0 and c_0. For the same reason, the material derivative D/Dt is replaced by $\partial/\partial t$.

Similarly, during the high Reynolds number entry of the train nose into the tunnel and hood the influence of vorticity production at the surfaces of the train and at the tunnel and hood walls is initially small. Therefore the vortex source on the right of Eq. (1) can also be discarded and the equation reduced to

$$\left(\frac{1}{c_0^2}\frac{\partial^2}{\partial t^2}-\nabla^2\right)B=0. \tag{2}$$

This equation is valid in the air bounded by the interior and exterior surfaces of the tunnel and hood and by the moving surface of the train. The latter is acoustically equivalent to surface distributions of monopole and dipole sources [18]. The monopoles account for the massive displacement of the air ahead of the advancing train. The dipoles correspond to the reaction force on the train arising from the pressure rise over the nose within the hood and tunnel. Howe et al. [21] obtained a slender body approximation for these sources, and showed that the surface of the moving train could be ignored provided these equivalent sources are inserted on the right of Eq. (2), which then assumes the form

$$\left(\frac{1}{c_0^2}\frac{\partial^2}{\partial t^2}-\nabla^2\right)B=\frac{U}{(1-M^2)}\left(1+\frac{\mathcal{A}_0}{\mathcal{A}}\right)\frac{\partial}{\partial t}\left(\frac{\partial \mathcal{A}_T}{\partial x}(x+Ut)\delta(y)\delta(z)\right), \tag{3}$$

where $M = U/c_0$ is the train Mach number. In this equation $\mathcal{A}_T(s)$ is the cross-sectional area of the train (which is constant except over the nose and tail regions), where s is distance measured from the tip of the nose, which is assumed to enter the hood (x=0) at time t = 0. The approximation replaces the surface monopoles and dipoles by a line source on the train axis extending over the interval $-Ut<x<L-Ut$ occupied by the nose of length L at time t, and is applicable provided the *blockage* $\mathcal{A}_0/\mathcal{A}$ is less than about 0.2 and $M\le 0.4$. The term involving the factor $\mathcal{A}_0/\mathcal{A}$ in (3) accounts for the contribution from the dipoles.

2.3. Green's function

Eq. (3) will be solved by Green's function method described in [26] for a hood that has uniform cross-sectional area except possibly near its inner, junction end (Fig. 5). Green's function $G(\mathbf{x},\mathbf{x}';t-\tau)$ is the causal solution of (3) when the right hand side is replaced by the point source $\delta(\mathbf{x}-\mathbf{x}')\delta(t-\tau)$ at position $\mathbf{x}=\mathbf{x}'$ and time $t=\tau$. It is required to have vanishing normal derivative on the rigid walls of the tunnel and hood. The characteristic thickness of the unmodified compression wavefront $\sim 2R/M$ [18,26], so that the tunnel radius is acoustically compact. In these circumstances it was shown in [26] for a hood of overall length $\ell_h \gg R$ that

$$G(\mathbf{x},\mathbf{x}';t-\tau)=\frac{c_0\mathcal{T}_J}{2\mathcal{A}_h}\sum_{n=0}^{\infty}\mathcal{R}_E^n\mathcal{R}_J^n\left\{\mathrm{H}\left([t]-\tau-\frac{(2n\ell+\varphi^*(\mathbf{x}'))}{c_0}\right)+\mathcal{R}_E\mathrm{H}\left([t]-\tau-\frac{(2n\ell-\varphi^*(\mathbf{x}'))}{c_0}\right)\right\},\quad \ell=\ell_h+\ell', \tag{4}$$

provided the observer position $\mathbf{x}$ lies within the tunnel at distances $|x+\ell_h|\gg R$ from the junction of the hood and tunnel.

In this formula $\mathrm{H}(\cdot)$ denotes the Heaviside step function, and $[t]=t+(x-\ell')/c_0$ is a retarded time (the delay required for sound to travel outward from the source) involving the end correction $\ell'\approx 0.61R_h$ of the open end of the hood [25,27]. The coefficients $\mathcal{R}_E,\mathcal{R}_J$ and $\mathcal{T}_J$ are defined by reference to Fig. 4 in terms of the cross-sectional areas of the tunnel and hood by

$$\mathcal{R}_E=-1,\quad \mathcal{R}_J=\frac{\mathcal{A}_h-\mathcal{A}}{\mathcal{A}_h+\mathcal{A}},\quad \mathcal{T}_J=\frac{2\mathcal{A}_h}{\mathcal{A}_h+\mathcal{A}}. \tag{5}$$

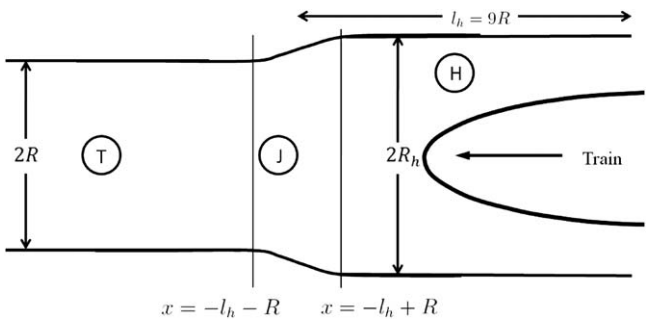

Fig. 4. Axisymmetric tunnel and hood with sections T, J, H, and E, respectively, designating the tunnel, junction, hood body, and hood entrance sections. Junction boundaries are at $x=-l_h-R,\ -l_h+R$.

For a plane sound wave of wavelength $\gg R$, $\mathcal{R}_J$ is the reflection coefficient for reflection back into the hood at the junction J of the tunnel and hood; $\mathcal{R}_E$ is the corresponding reflection coefficient at the open end E, and $\mathcal{T}_J$ is the transmission coefficient for transmission at J from the hood into the tunnel.

The function φ^* is a velocity potential that satisfies Laplace's equation and the following conditions:

$$\varphi^*(\mathbf{x}) \sim \begin{cases} x-\ell' & \text{when } |x| \gg R_h \text{ in the region H within the hood,} \\ -\mathcal{A}_h/4\pi|\mathbf{x}| & \text{when } |\mathbf{x}| \gg R_h \text{ in the region outside of the hood.} \end{cases} \tag{6}$$

When $\ell_h \gg R_h$ the functional form of φ^* in the vicinity of the open end E coincides with the corresponding potential φ^*_E of a flow from a semi-infinite circular cylinder of radius R_h. The latter is known in analytic form [23], and the relevant formulae for our needs are

$$\varphi^*(\mathbf{x}) \equiv \varphi^*_E(\mathbf{x}) \quad \text{in region E} \tag{7}$$

where

$$\frac{\partial \varphi^*_E}{\partial x}(\mathbf{x}) = \frac{1}{2} - \frac{1}{2\pi}\int_0^\infty \mathrm{I}_0\left(\frac{\xi r}{R_h}\right)\left(\frac{2\mathrm{K}_1(\xi)}{\mathrm{I}_1(\xi)}\right)^{1/2} \sin\left\{\xi\left(\frac{x}{R_h}+\mathcal{Z}(\xi)\right)\right\}\mathrm{d}\xi, \quad r=\sqrt{y^2+z^2},$$

$$\mathcal{Z}(\xi) = \frac{1}{\pi}\int_0^\infty \ln\left(\frac{\mathrm{K}_1(\mu)\mathrm{I}_1(\mu)}{\mathrm{K}_1(\xi)\mathrm{I}_1(\xi)}\right)\frac{\mathrm{d}\mu}{\mu^2-\xi^2}, \tag{8}$$

in which I_0, I_1 and K_1 are modified Bessel functions.

Similarly, in the neighborhood of the junction region J we can put

$$\varphi^*(\mathbf{x}) = \frac{\mathcal{A}_h}{\mathcal{A}}\varphi^*_J(\mathbf{x}) - \ell, \quad \ell = \ell_h + \ell', \tag{9}$$

where to an excellent approximation $\varphi^*_J(\mathbf{x})$ is the velocity potential of an incompressible flow in the x-direction through the region J connecting two *semi-infinite* cylindrical ducts of radius R, R_h, respectively, and where

$$\begin{aligned} \varphi^*_J(\mathbf{x}) &\sim x+\ell_h-\ell_j \quad \text{when } |x+\ell_h| \gg R \text{ in the region T of the tunnel,} \\ &\sim \frac{\mathcal{A}}{\mathcal{A}_h}(x+\ell_h) \text{when } |x+\ell_h| \gg R_h \text{ in the region H of the hood.} \end{aligned} \tag{10}$$

The length $\ell_j \ll R$ is an effective end correction of the transition region J, which is small enough to be neglected [26]. The detailed behavior of $\varphi^*_J(\mathbf{x})$ is easily obtained using a routine finite difference approximation to the potential flow equation within the region J connecting the circular cylindrical tunnel to a nominally semi-infinite circular cylindrical hood (details are discussed in [28]).

2.4. Calculation of the compression wave

In the acoustic region within the tunnel and ahead of the train, the unsteady component of the pressure $p \simeq \rho_0 B$, where B is the solution of Eq. (3). A formula for the corresponding pressure gradient $\partial p/\partial t$ is obtained by differentiation of the convolution of $G(\mathbf{x},\mathbf{x}';t-\tau)$ defined by Eq. (4) and the source on the right of Eq. (3), i.e.

$$\frac{\partial p}{\partial t}(\mathbf{x},\, t) = \frac{\rho_0 U}{(1-M^2)}\left(1+\frac{\mathcal{A}_0}{\mathcal{A}}\right)\frac{\partial^2}{\partial t^2}\int\int_\infty^\infty \frac{\partial \mathcal{A}_T}{\partial x'}(x'+U\tau)G(\mathbf{x},x',0,0;t-\tau)\,\mathrm{d}x'\,\mathrm{d}\tau. \tag{11}$$

Because of the identity

$$\frac{\partial \mathcal{A}_T}{\partial t}(x+Ut) = U\frac{\partial \mathcal{A}_T}{\partial x}(x+Ut)$$

and by integration by parts, we can also write

$$\frac{\partial p}{\partial t} = \frac{\rho_0 U^3}{(1-M^2)}\left(1+\frac{\mathcal{A}_0}{\mathcal{A}}\right)\iint_{-\infty}^\infty \frac{\partial \mathcal{A}_T}{\partial x'}(x'+U\tau)\frac{\partial^2 G}{\partial x'^2}(\mathbf{x},x',0,0;t-\tau)\,\mathrm{d}x'\,\mathrm{d}\tau. \tag{12}$$

When the Mach number is small the second derivative $\partial^2 G/\partial x'^2$ can be evaluated using the approximation

$$\frac{\partial^2 \mathrm{H}}{\partial x'^2}\left([t]-\tau-\frac{(2n\ell \pm \varphi^*(\mathbf{x}'))}{c_0}\right) \approx \mp\frac{1}{c_0}\frac{\partial^2 \varphi^*}{\partial x'^2}(\mathbf{x}')\delta\left([t]-\tau-\frac{(2n\ell \pm \varphi^*(\mathbf{x}'))}{c_0}\right), \tag{13}$$

the term omitted on the right hand side being $\mathrm{O}(M)$ smaller.

The function $\partial^2\varphi^*/\partial x'^2$ is nonzero only in the immediate vicinities of the hood open end and within the transition region J, where it is defined by Eqs. (8) and (9) and, respectively, $\varphi^* \simeq 0, -\ell$. Hence

$$\frac{\partial p}{\partial t} = \frac{-\rho_0 U^3}{\mathcal{A}_h(1-M^2)}\left(1+\frac{\mathcal{A}_0}{\mathcal{A}}\right)\mathcal{T}_J\sum_{n=0}^{\infty}(-1)^n\mathcal{R}_J^n\int_{-\infty}^{\infty}\frac{\partial \mathcal{A}_T}{\partial x'}(x'+U[t]-2nM\ell)\frac{\partial^2\varphi_E^*}{\partial x'^2}(x',0,0)\,\mathrm{d}x'$$
$$-\frac{\rho_0 U^3}{2\mathcal{A}(1-M^2)}\left(1+\frac{\mathcal{A}_0}{\mathcal{A}}\right)\mathcal{T}_J\sum_{n=0}^{\infty}(-1)^n\mathcal{R}_J^n\int_{-\infty}^{\infty}\left\{\frac{\partial \mathcal{A}_T}{\partial x'}(x'+U[t]-(2n-1)M\ell)+\frac{\partial \mathcal{A}_T}{\partial x'}(x'+U[t]-(2n+1)M\ell)\right\}\frac{\partial^2\varphi_J^*}{\partial x'^2}(x',0,0)\,\mathrm{d}x'. \tag{14}$$

Successive terms in these expansions account for partial wave contributions to $\partial p/\partial t$ from interactions between the train nose and the portal E and junction J, and the subsequent effects of multiple reflections of these waves from the ends of the hood. For the applications discussed in this paper it is assumed that $R_h/R=1.25$ and $\ell \sim 10R$, which are typical of newer full scale tunnels and hoods. Then $\mathcal{R}_J \approx 0.22$ and $\mathcal{T}_J \approx 1.22$, and the higher order terms decrease rapidly. In any event, we shall be concerned in practice with nondimensional retarded times $U[t]/R$ no larger than about 20, for which it is necessary to take account of at most three round trip reflections between the ends of the hood. This means that it is sufficient to replace the general expression (14) by the truncated formula

$$\frac{\partial p}{\partial t} = \frac{-\rho_0 U^3}{\mathcal{A}(1-M^2)}\left(1+\frac{\mathcal{A}_0}{\mathcal{A}}\right)\mathcal{T}_J\left\{\frac{\mathcal{A}}{\mathcal{A}_h}\int_{-\infty}^{\infty}[\mathcal{A}_T'(x'+U[t])-\mathcal{R}_J\mathcal{A}_T'(x'+U[t]-2M\ell)+\mathcal{R}_J^2\mathcal{A}_T'(x'+U[t]-4M\ell)\right.$$
$$-\mathcal{R}_J^3\mathcal{A}_T'(x'+U[t]-6M\ell)]\frac{\partial^2\varphi_E^*}{\partial x'^2}(x',0,0)\,\mathrm{d}x'+\frac{1}{2}\int_{-\infty}^{\infty}[\mathcal{A}_T'(x'+U[t]+M\ell)+(1-\mathcal{R}_J)\mathcal{A}_T'(x'+U[t]-M\ell)$$
$$\left.-\mathcal{R}_J(1-\mathcal{R}_J)\mathcal{A}_T'(x'+U[t]-3M\ell)]\frac{\partial^2\varphi_J^*}{\partial x'^2}(x',0,0)\,\mathrm{d}x'\right\}, \tag{15}$$

where $\mathcal{A}_T'$ designates the derivative of $\mathcal{A}_T$ with respect to x'.

Eqs. (14) and (15) demonstrate that the shape of the pressure gradient wave is determined principally by the train nose profile, and by the geometries of the hood portal and the transition region J (which determine the functional forms of $\partial^2\varphi_E^*/\partial x^2$ and $\partial^2\varphi_J^*/\partial x^2$).

3. Predictions for a uniform hood

Predictions of Eq. (15) have been validated for an unmodified hood of uniform cross section by comparison with model scale test results obtained at the Railway Technical Research Institute in Tokyo [26]. The tunnel consisted of a 7 m long circular cylindrical tube made of hard vinyl chloride, with inner and outer diameters respectively equal to 10 and 11.4 cm. The hood was 50 cm long (so that $\ell_h = 10R$) and had inner and outer diameters respectively equal to 12.5 and 13.1 cm; a 10 cm long collar provided an airtight join between the tunnel and hood. Each of the model trains used in the tests was constructed of a nylon plastic material with the radius of the cylindrical, uniform section of the train equal to $h=2.235$ cm. The train nose (and also the 'tail') was ellipsoidal and of axial length L, obtained by rotating the curve $y = h\sqrt{(x/L)(2-x/L)}$, $0 < x < L$ about the x-axis. The cross-sectional area $\mathcal{A}_T(x)$ of the forward part of the train at distance x from the nose tip is given by

$$\frac{\mathcal{A}_T(x)}{\mathcal{A}_0} = \begin{cases} \dfrac{x}{L}\left(2-\dfrac{x}{L}\right), & 0 < x < L, \\ 1, & x > L, \end{cases} \tag{16}$$

where the area of the uniform section $\mathcal{A}_0 = \pi h^2 = 15.69\,\mathrm{cm}^2$, so that the blockage is $\mathcal{A}_0/\mathcal{A} = 0.2$.

Results were reported in [26] for two model trains (i) and (ii) with different nose aspect ratios L/h detailed in Table 1. A friction drive 'launcher' involving three pairs of vertically aligned wheels was used to project the train into the tunnel along a 5.5 mm diameter steel wire extending along the common axis of the tunnel and hood. The maximum attainable speed was about 450 km/h, the actual speed being controlled by varying the rates of rotation of the wheels. A 3.75 m long open section between the launcher and the hood ensured that spherically spreading pressure waves generated during acceleration from the launcher are negligible at the hood portal. Two wall-mounted transducers measured the acoustic pressure p at two locations within the tunnel, the first at 1.5 m from the hood entrance and the second at 2.5 m. The pressure was recorded continuously until the rarefaction wave produced by the reflection of the compression wave at the far end of the tunnel is first detected by the second transducer. The pressure gradient $\partial p/\partial t$ was then calculated

Table 1
Specifications of the model trains.

Train	Nose length L (cm)	Aspect ratio L/h	Overall length (cm)	Total mass (g)
(i)	11.18	5.0	124.3	920
(ii)	6.70	3.0	92.0	640

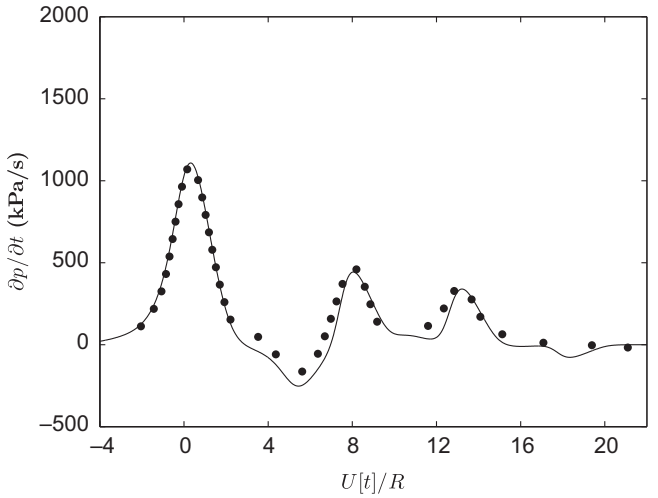

Fig. 5. Comparison between experimental results (•••) and analytical results (—) of Eq. (15) at train speed 294 km/h for the train nose profile (16).

after the removal of high frequency components (> 1 kHz) of the measured pressure using a fast Fourier transform algorithm.

A comparison of the predictions of Eq. (15) and measurements for train model (i) are displayed in Fig. 5 for U = 294 km/h. The pressure gradient is plotted as a function of the non-dimensional retarded time $U[t]/R$ where t is measured from the instant at which the train nose enters the hood. The agreement between theory and experiment is good, demonstrating the soundness of the theory. Equally good agreement between theory and experiment was reported in [26] for the short nosed train model (ii), and also in [18] for different train speeds and nose profiles.

3.1. Analysis of the pressure gradient profile

The subjective impact of the compression wave is determined predominantly by the peaks of the pressure gradient profile. The magnitudes and positions of the first three peaks are governed by the various terms in the truncated expansion (15) for $\partial p/\partial t$. Thus, the component

$$\mathcal{A}_T'(x'+U[t])\frac{\partial^2\varphi_E^*}{\partial x'^2}(x',0,0)$$

of the first integrand determines the first or principal peak at $U[t]/R \simeq 0$, generated as the nose enters the open end of the hood. Indeed, $\partial^2\varphi_E^*/\partial x'^2$ vanishes everywhere except near the hood entrance at $x'=0$ and $\mathcal{A}_T'(x'+U[t])$ is nonzero only at the retarded position of the nose where $x'+U[t]\sim 0$, so the product is finite only near $U[t]/R=0$. The remaining terms in the first integrand of (15) alternate in sign and correspond to the respective arrivals at $U[t]/R \simeq 2M\ell/R$, $4M\ell/R$, $6M\ell/R$ of the first, second, and third 'round trip' reflections of the principal peak from the ends of the hood; they decrease rapidly in magnitude because $\mathcal{R}_J \ll 1$.

The integrand in the second integral on the right of Eq. (15) vanishes everywhere except near $x'=-\ell_h$, at the junction between the hood and tunnel (the only region where $\partial^2\varphi_J^*/\partial x'^2 \neq 0$). A positive pulse is radiated into the tunnel and an equal negative pulse is radiated back towards the hood entrance when the front of the train crosses the junction at time $t\sim \ell_h/U$. The first term in this second integral is therefore responsible for the second peak of $\partial p/\partial t$ shown in Fig. 5 near $U[t]/R=(\ell_h-M\ell)/R\sim 7.5$.

The second term in the second integrand on the right of (15) can be split into the two components:

$$\mathcal{A}_T'(x'+U[t]-M\ell)\frac{\partial^2\varphi_J^*}{\partial x'^2}(x',0,0)-\mathcal{R}_J\mathcal{A}_T'(x'+U[t]-M\ell)\frac{\partial^2\varphi_J^*}{\partial x'^2}(x',0,0).$$

The first represents the contribution from the negative junction pulse after reflection from the hood entrance, whereas the second term is a second contribution from the positive junction pulse, part of which is reflected at the junction and again at the open end of the hood. Together these waves produce a third peak at $U[t]/R \simeq (\ell_h+M\ell)/R\sim 12.5$, with an amplitude which is smaller than the second peak radiated from the junction by a factor approximately equal to $1-\mathcal{R}_J \approx 0.78$.

The final term in the second integrand produces a small depression in $\partial p/\partial t$ at $U[t]/R \simeq (\ell_h+3M\ell)/R\sim 17.5$, which is not relevant in the present discussion because its modification will not make any significant change to the pressure gradient.

4. Optimization of the hood-tunnel junction

The magnitude of the principal peak of the compression wave pressure gradient $\partial p/\partial t$ depends on the geometry of the hood open end and on the area contraction ratio at the junction with the tunnel. It is not affected by the details of the transition between the hood and tunnel, provided this occurs over an acoustically compact axial distance. The secondary peaks are produced by scattering of the train near-field at the junction, and therefore can conceivably be modified by making suitable changes to the tunnel wall profile across the transition region. We now determine the optimal form of these changes that provide an overall minimization of these secondary peaks for train speeds U in the range 250–350 km/h.

Numerical results will be presented for hoods with a nominal length $\ell_h = 9R$, and for $R_h/R = 1.25$, although these values in no way limit the generality of our proposed method. A schematic of the continuously variable tunnel-hood geometry is illustrated in Fig. 4. Green's function (4) and the formal representation (15) are valid provided the axial width of the transition region is small compared to the characteristic thickness of the compression wave ($> 2R/M$, where $M \leq 0.3$ when U does not exceed 350 km/h). We shall therefore assume that the transition region occupies an axial distance no larger than $2R$ within the interval $-\ell_h - R < x < -\ell_h + R$, wherein the transition wall profile has the general functional form

$$r = f(x), \quad -R < x + \ell_h < +R, \tag{17}$$

subject to the constraints $f(-\ell_h - R) = R$, $f(-\ell_h + R) = R_h$. The overall hood length including the transition region $\approx 10R$, and it is therefore appropriate to compare predictions with the uniform (unmodified) hood discussed in Section 3, for which

$$f(x) = R + (R_h - R)\mathrm{H}(x + 10R).$$

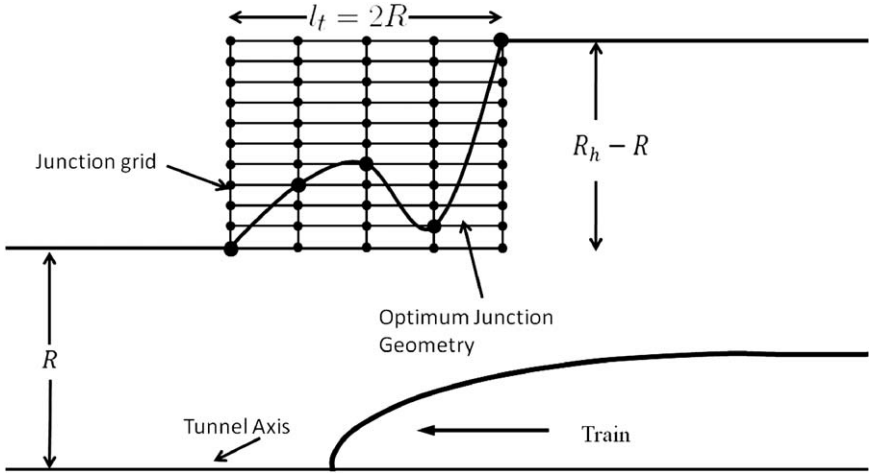

Fig. 6. Illustration of the optimum tunnel configuration for train (i) and the grid used to obtain it.

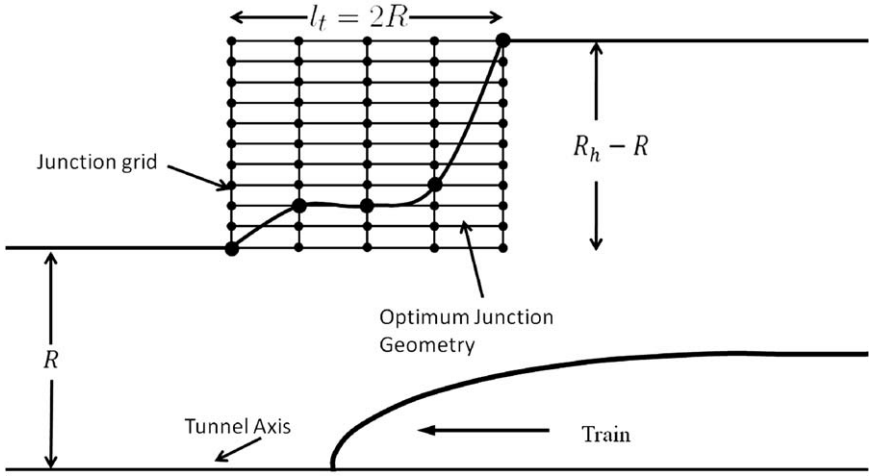

Fig. 7. Illustration of the optimum tunnel configuration for train (ii) and the grid used to obtain it.

Table 2
Optimal grid nodes for trains (i) and (ii) at U=300 km/h.

n	x_n/R	r_n/R, model (i)	r_n/R, model (ii)
1	−10	1	1
2	−9.5	1.075	1.050
3	−9.0	1.100	1.050
4	−8.5	1.050	1.075
5	−8.0	1.250	1.250

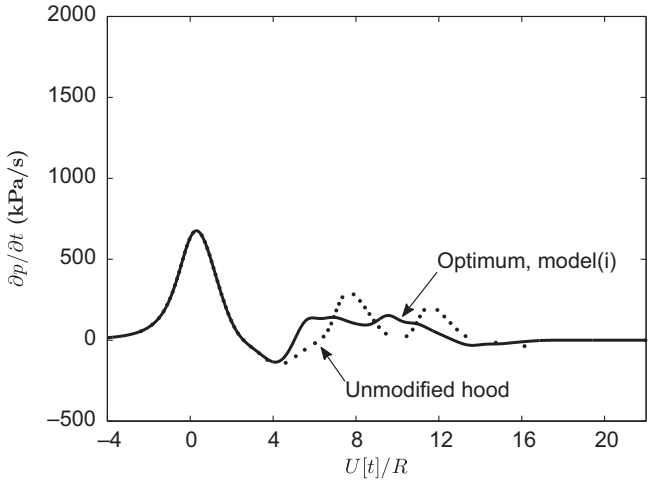

Fig. 8. Predicted pressure gradient for U=250 km/h and train model (i): (•••) uniform hood of length 9R; (—) optimized hood.

Each of the candidate transition profiles $r=f(x)$ is defined by selecting a set of five nodal points (x_n,r_n), $1\le n\le 5$, of a rectangular grid that spans the domain $(-R<x+\ell_h<R,\ R<r<R_h)$ of the (x,r)-plane, where $x_n=-\ell_h+(n-3)R/2 \equiv (n-21)R/2$ and $r_1 = R$, $r_5 = R_h$. Fig. 8 illustrates the 5×11 grid used in the computations, the nodal interval in the radial direction being $(R_h-R)/10\equiv 0.025R$. There are $11^3 = 1331$ possible nodal sets, each of which is used to define $f(x)$ as a smooth function passing through the five nodes and determined elsewhere by a conventional third-order spline approximation. For each nodal set Laplace's equation was solved numerically to determine the corresponding velocity potential $\varphi_J^*(\mathbf{x})$ defining flow through the junction. The compression wave pressure gradient was then calculated using Eq. (15) for the train speed U = 300 km/h. The optimal nodal set and transition function $f(x)$ were defined by the condition that the sum of the second and third peak values of $\partial p/\partial t$ should be a minimum. This set was also found to be optimal at speeds U = 250, 350 km/h. The optimal transition profiles for the long and short nosed trains (i) and (ii) are found to be different and are plotted in Figs. 6 and 7. The corresponding grid nodes defining $f(x)$ are given in Table 2. The optimal functional forms of $f(x)$ were found to be very similar to those displayed in the figures when the calculations were repeated using a coarser 5×6 grid.

5. Discussion of the numerical results

5.1. Long-nosed train model (i)

The predicted optimal pressure gradient $\partial p/\partial t$ for train model (i) is plotted (—) in Figs. 8, 9 and 10, respectively, for U = 250, 300, 350 km/h; the corresponding plots for the uniform (unmodified) hood are also shown (• • •). There is a strong dependence on U because $\partial p/\partial t\propto U^3$: when U increases from 250 to 300 km/h the magnitude of the principal peak increases by about 70%, and by about 60% for an increase from 300 to 350 km/h. The optimized junction yields a significant reduction in the magnitude of the second and third peaks relative to those for a uniform hood at all three train speeds. At 250 km/h the magnitudes of the second and third peaks decrease by $\sim$30% and $\sim$20%, respectively. At 300 km/h the reduction is more dramatic: more than 70% for the second peak while still reducing the third peak by about 15%. The effectiveness of the optimum transition profile tends to decrease at higher speeds. At 350 km/h the second and third peaks are reduced only by $\sim$30%.

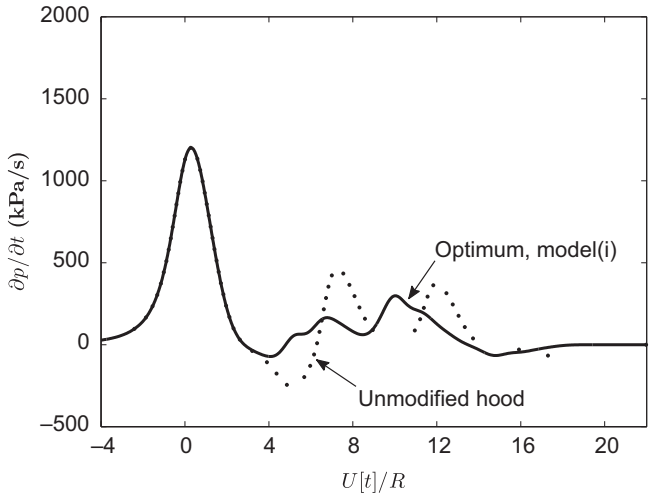

Fig. 9. Predicted pressure gradient for U=300 km/h and train model (i): (•••) uniform hood of length 9R; (—) optimized hood.

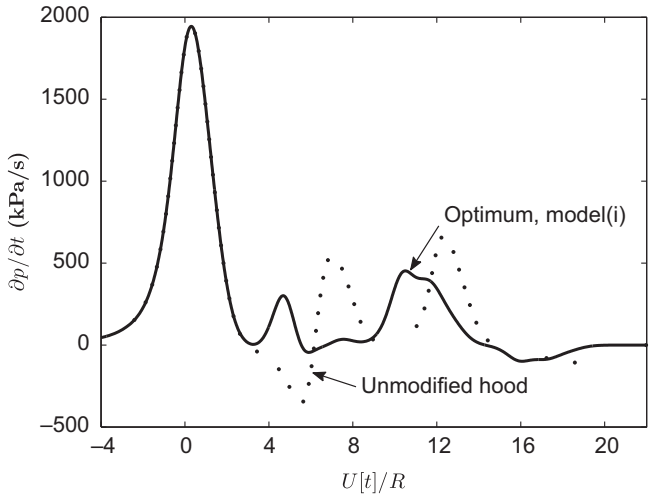

Fig. 10. Predicted pressure gradient for U=350 km/h and train model (i): (•••) uniform hood of length 9R; (—) optimized hood.

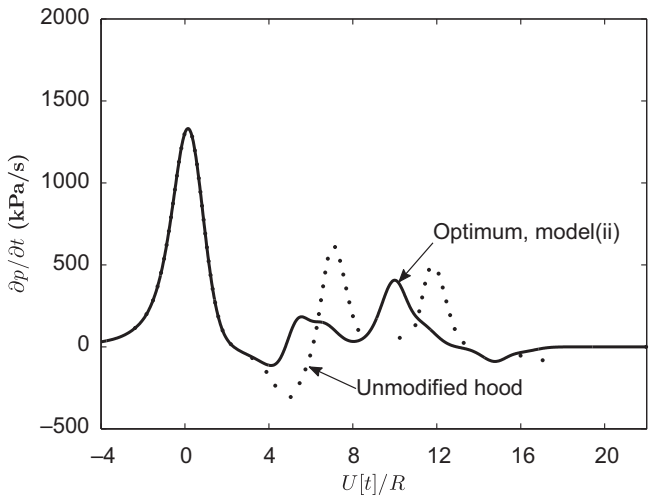

Fig. 11. Predicted pressure gradient for U=300 km/h and train model (ii): (•••) uniform hood of length 9R; (—) optimized hood.

5.2. Short-nosed train model (ii)

The corresponding pressure gradient plots for train model (ii) are shown in Fig. 11 for U = 300 km/h. The effects of speed are similar in this case to those noted for train model (i). A significant reduction in the magnitudes of the second and third peaks relative to those for the unmodified, uniform hood is found at all three train speeds. At 300 km/h the second and third peaks are respectively reduced by more than 60% and by $\sim 30\%$.

It is also of interest to examine the effect on the secondary peaks of $\partial p/\partial t$ when train model (ii) enters the hood optimized for train (i), and vice versa. Fig. 12 compares the pressure gradient profile for both trains entering the hood optimized for the long nosed model (i) at U=300 km/h. Both secondary peaks of the pressure gradient for model (ii) are increased by about 15% relative to model (i) because of its the shorter nose. Fig. 13 depicts the pressure gradient profiles when the trains enter the hood optimized for the short nosed model (ii), again at U=300 km/h. In this case the primary and secondary peaks of $\partial p/\partial t$ for model (i) are seen to be smaller than the corresponding peaks for model (ii) because of its increased the nose length, and are actually comparable to the pressure gradient peaks produced when model (i) enters the hood optimized for its own geometry. Therefore, if in practice both long and short nosed trains are required to use the same hood, it is recommended that the hood geometry be optimized for the short nose.

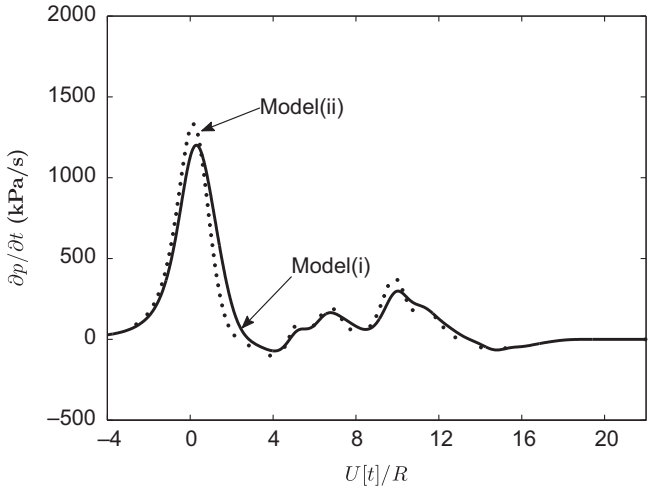

Fig. 12. Predicted pressure gradient for U=300 km/h and train models (i) (—) and (ii) (•••) entering hood optimized for train model (i).

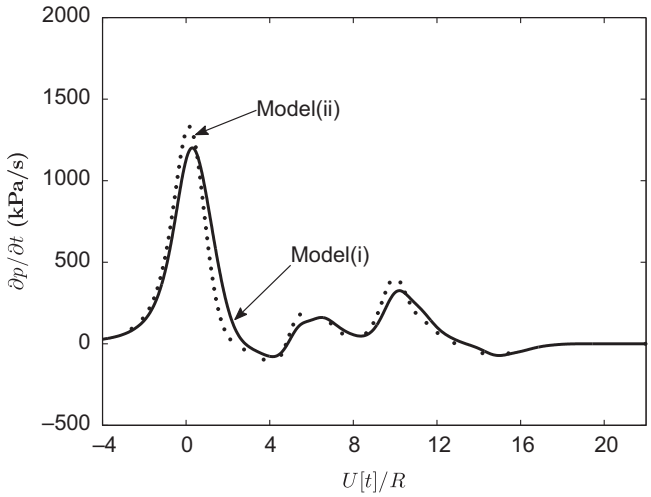

Fig. 13. Predicted pressure gradient for U=300 km/h and train models (i) (—) and (ii) (•••) entering hood optimized for train model (ii).

6. Conclusion

When a high-speed train enters a long tunnel having no hood the compression wave produced in the tunnel is attributed to the interaction of the train nose with the tunnel entrance portal. The resulting micro-pressure wave radiated from the distant exit, possibly exacerbated by nonlinear steepening during propagation in the tunnel, consists of a single, loud, pulsatile 'bang'. On the other hand, when the train enters via an unvented hood of uniform cross-section $\mathcal{A}_h$ larger than the tunnel cross-section $\mathcal{A}$, the compression wave has a more complex structure that includes components generated by interactions and reflections at both the hood portal and at the junction of the tunnel and hood. These transform what would otherwise be a rapidly rising compression wavefront into an elongated pressure rise with superimposed ripples, and the corresponding loud 'bang' can be expected to be attenuated into a series of quieter 'claps'.

The ripples produce a micro-pressure wave that consists of a principal peak followed by secondary peaks of diminishing magnitudes. The amplitude of the principal peak is determined by the interaction of the train nose with the hood portal (modified by nonlinear steepening), and can only be reduced by modification of the geometry of the hood entrance. The amplitudes of the secondary peaks are governed predominantly by the hood-tunnel wall profile within the transition region between the hood and the tunnel. We have shown how the wall in the transition region can be optimally profiled to minimize the amplitudes of the secondary peaks. The optimized transition geometry depends both on train speed and on the train nose aspect ratio. Our numerical results indicate that the optimal geometry is most effective at $U \sim 300\,\mathrm{km/h}$, when the second peak is typically about 70% smaller than that for a uniform hood for which the transition from $\mathcal{A}_h$ to $\mathcal{A}$ occurs 'discontinuously' at the junction. It becomes less effective at higher speeds. For operations involving both long and short nosed trains we have also shown that the junction should be optimized for the shorter nose, because the attenuation achieved for the longer nosed train is then close to optimal. We realize the difficulties involved in building the optimal geometry; any proposed construction would of course require approximations to this shape.

References

[1] W. Tollmien, Drag and pressure variations occurring as a train passes through a tunnel, *Zeitschrift des Vereines Deutscher Ingenieure* 71 (6) (1927) 199–203 (in German).

[2] T. Hara, Aerodynamic force acting on a high speed train at tunnel entrance, *Bulletin of the Japan Society of Mechanical Engineers* 4 (1961) 547–553.

[3] T. Hara, M. Kawaguti, G. Fukuchi, A. Yamamoto, Aerodynamics of high-speed train, *Monthly Bulletin of the International Railway Congress Association* XLV (2) (1968) 121–146.

[4] W.A. Woods, C.W. Pope, Secondary aerodynamic effects in rail tunnels during vehicle entry, *Second BHRA Symposium of the Aerodynamics and Ventilation of Vehicle Tunnels*, Cambridge, England, 23–25 March 1976, Paper C5, 1976, pp. 71–86.

[5] S. Ozawa, Y. Morito, T. Maeda, M. Kinosita, Investigation of the pressure wave radiated from a tunnel exit, *Railway Technical Research Institute Report* No. 1023, 1976 (in Japanese).

[6] R.G. Gawthorpe, Aerodynamics of trains in tunnels, *Railway Engineer International* 3 (4) (1978) 41–47.

[7] S. Ozawa, T. Maeda, Tunnel entrance hoods for reduction of micro-pressure wave, *Quarterly Report of the Railway Technical Research Institute* 29 (3) (1988) 134–139.

[8] S. Ozawa, T. Maeda, T. Matsumura, K. Uchida, H. Kajiyama, K. Tanemoto, Countermeasures to reduce micro-pressure waves radiating from exits of Shinkansen tunnels, in: A. Haerter (Ed.), *Aerodynamics and Ventilation of Vehicle Tunnels*, Elsevier Science Publishers, 1991, pp. 253–266.

[9] T. Maeda, T. Matsumura, M. Iida, K. Nakatani, K. Uchida, Effect of shape of train nose on compression wave generated by train entering tunnel, in: M. Iguchi (Ed.), *Proceedings of the International Conference on Speedup Technology for Railway and Maglev Vehicles*, Yokohama, Japan, 22–26 November 1993, 1993, pp. 315–319.

[10] M. Iida, T. Matsumura, K. Nakatani, T. Fukuda, T. Maeda, Optimum nose shape for reducing tunnel sonic boom, *Institution of Mechanical Engineers Paper* C514/015/96, 1996.

[11] R. Gregoire, J. M. Rety, V. Moriniere, M. Bellenoue, T. Kageyama, Experimental study (scale 1/70th) and numerical simulations of the generation of pressure waves and micro-pressure waves due to high-speed train-tunnel entry, in: J.R. Gillard (Ed.), *Proceedings of the 9th International Conference on Aerodynamics and Ventilation of Vehicle Tunnels*, Aosta Valley, Italy, 6–8 October 1997, ME Publications, London, pp. 877–902.

[12] K. Matsuo, T. Aoki, S. Mashimo and E. Nakatsu, Entry compression wave generated by a high-speed train entering a tunnel, in: J.R. Gillard (Ed.), *Proceedings of the 9th International Conference on Aerodynamics and Ventilation of Vehicle Tunnels*, Aosta Valley, Italy, 6–8 October 1997, ME Publications, London, pp. 925–934.

[13] J.L. Peters, Tunnel optimized train nose shape, Paper presented at the *10th International Symposium on Aerodynamics and Ventilation of Vehicle Tunnels*, Boston, USA, 1–3 November 2000.

[14] T. Maeda, Micropressure waves radiating from a Shinkansen tunnel portal, in: V.V. Krylov, T. Telford (Eds.), *Noise and Vibration from High Speed Trains*, 2002 (Chapter 7).

[15] T. Maeda, Japanese Shinkansen noise: Development of noise reduction technology, Paper presented at *Inter-Noise 2006*, 3–6 December, Honolulu, Hawaii.

[16] S. Ozawa, T. Uchida, T. Maeda, Reduction of micro-pressure wave radiated from tunnel exit by hood at tunnel entrance, *Quarterly Report of the Railway Technical Research Institute* 19 (2) (1978) 77–83.

[17] S. Ozawa, T. Maeda, Model experiment on reduction of micro-pressure wave radiated from tunnel exit, in: R.I. Emori (Ed.), *Proceedings of the International Symposium on Scale Modeling*, Tokyo, 18–22 July 1988. Seikei University, Japan Society of Mechanical Engineers, pp. 33–37.

[18] M.S. Howe, M. Iida, T. Maeda, Y. Sakuma, Rapid calculation of the compression wave generated by a train entering a tunnel with a vented hood, *Journal of Sound and Vibration* 297 (2006) 267–292.

[19] A.E. Vardy, Reflection of step-wavefronts from perforated and flared extensions, *Journal of Sound and Vibration* 59 (1978) 577–589.

[20] J. Anthoine, Alleviation of the pressure rise from a high-speed train entering a tunnel, *American Institute of Aeronautics and Astronautics Journal* 47 (2009) 2132–2142.

[21] M.S. Howe, M. Iida, T. Fukuda, T. Maeda, Theoretical and experimental investigation of the compression wave generated by a train entering a tunnel with a flared portal, *Journal of fluid Mechanics* 425 (2000) 111–132.

[22] A. Winslow, M.S. Howe, M. Iida, Influence of a scarfed portal on the compression wave generated by a high-speed train entering a tunnel, *Journal of Low Frequency Noise, Vibration and Active Control* 24 (2005) 203–217.

[23] M.S. Howe, The compression wave produced by a high-speed train entering a tunnel, *Proceedings of the Royal Society A* 454 (1998) 1523–1534.

[24] M.S. Howe, M. Iida, Influence of separation on the compression wave generated by a train entering a tunnel, *International Journal of Aeroacoustics* 2 (2003) 13–33.
[25] M.S. Howe, *Acoustics of Fluid–Structure Interactions*, Cambridge University Press, Cambridge, 1998.
[26] M.S. Howe, M. Iida, T. Fukuda, Influence of an unvented tunnel entrance hood on the compression wave generated by a high-speed train, *Journal of Fluids and Structures* 17 (2003) 833–853.
[27] L. Rayleigh, *The Theory of Sound*, vol. 2, Macmillan, London, 1926.
[28] P. R. Murray, *Influence of hood geometry on the compression wave generated by a high speed train*, MS Thesis, Boston University, Department of Mechanical Engineering, 2008.